



# Efficient Segmentation of Brain Tumor Using FL-SNM with a Metaheuristic Approach to Optimization

Aparna Natarajan<sup>1</sup> · Sathiyasekar Kumarasamy<sup>2</sup>

Received: 19 October 2018 / Accepted: 3 December 2018 / Published online: 2 January 2019  
© Springer Science+Business Media, LLC, part of Springer Nature 2019

## Abstract

Nowadays, automatic tumor detection from brain images is extremely significant for many diagnostic as well as therapeutic purposes, due to the unpredictable shape and appearance of tumors. In medical image analysis, the automatic segmentation of tumors from brain using magnetic resonance imaging (MRI) data is the most critical issue. Existing research has some limitations, such as high processing time and lower accuracy, because of the time required for the training process. In this research, a new automatic segmentation process is introduced using machine learning and a swarm intelligence scheme. Here, a fuzzy logic with spiking neuron model (FL-SNM) is proposed for segmenting the brain tumor region in MR images. Initially, input images are preprocessed to remove Gaussian and Poisson noise using a modified Kuan filter (MKF). In the MKF, the optimal selection of the minimum MSE of image pixels is achieved using a random search algorithm (RSA), which improves the peak signal-to-noise ratio (PSNR). Then, the image is smoothed using an anisotropic diffusion filter (ADF) to reduce the over-filtering problem. Afterwards, to extract statistical texture features, Fisher's linear-discriminant analysis (FLDA) is used. Finally, extracted features are transferred to the FL-SNM process and this scheme effectively segments the tumor region. In FL-SNM, the consequent parameters such as weight and bias play an important role in segmenting the region. Therefore, optimizing the weight parameter values using a chicken behavior-based swarm intelligence (CSI) algorithm, is proposed. The proposed (FL-SNM) scheme attained better performance in terms of high accuracy (94.87%), sensitivity (92.07%), specificity (99.34%), precision rate (89.36%), recall rate (88.39%), F-measure (95.06%), G-mean (95.63%), and DSC rate (91.2%), compared to existing convolutional neural networks (CNNs) and hierarchical self-organizing maps (HSOMs).

**Keywords** Kuan filter · Diffusion filter · Linear process · Optimization · Discriminant analysis · Fuzzy logic · Spiking neuron model · Swarm intelligence

## Introduction

In India, every year, over 40–50,000 persons are diagnosed with brain tumor; among these 20% are children who are suffering from medulloblastoma, which is a malignant pediatric brain tumor which spreads via the cerebro spinal fluid

(CSF) to various locations besides the surface of the brain and spinal cord (<http://timesofindia.indiatimes.com/life-style/health-fitness/health-news/Over-2500-Indian-kids-suffer-from-brain-tumour-every-xyear/articleshow/52714386.cms>).

Nowadays, diagnosing brain tumor is a challenging task due to the risk of complications in surgery. Segmenting the tumor area is possible for those diagnosed [1]. In recent years, the manual segmentation of the tumor region by a radiation oncologist has led to more time-consuming procedures, difficulties in segmenting the tumor region and mistreatment by experts, resulting in complications. The major complexities in segmentation are noise, bias field (smoothly varying intensities inside tissues) and the partial volume effect.

In manual segmentation, tumors can vary considerably in size, shape, position, and properties. In addition, the tumor has intensities that coincide with those of normal brain tissue. Frequently, the tumor deforms nearby healthy

This article is part of the Topical Collection on *Patient Facing Systems*

✉ Aparna Natarajan  
aparnan2101@gmail.com

Sathiyasekar Kumarasamy  
ksathiyasekar@gmail.com

<sup>1</sup> Department of EEE, SRS College of Engineering and Technology, Salem, India

<sup>2</sup> Department of EEE, S. A. Engineering College, Chennai, India

tissues if it expands, thus resulting in an abnormal size and shape.

To overcome these limitations, an automatic tumor segmentation method is developed for efficient tumor segmentation. The primary intention of this work is to develop an efficient automatic technique for image processing in a tumor segmentation system for brain MR images, with high accuracy [2]. It easily segments the tumor masses with high precision, robust diagnosis system and to attain better tumor detection efficiency.

In this research, MRI scanning images are used for tumor segmentation because this does not involve X-ray radiation and offers efficient detection. MRI is an extremely accurate method of disease detection and provides sufficient information to confirm a patient's diagnosis. It is a non-invasive and painless procedure. A method which uses magnetic signal to create images "slices" of the human body.

The automatic segmentation is achieved via three stages: preprocessing, feature extraction and segmentation [3]. Initially, the input image is preprocessed to reduce unwanted noise and to improve the PSNR for image quality and segmentation accuracy.

The preprocessed image is forwarded to the feature extraction system, to identify relevant features, such as shape, texture, and color, which contain more information used for segmentation. The extracted features are segmented by a neural network algorithm, to classify the tumor and non-tumor regions. A basic view of a brain tumor MR image is shown in Fig. 1.

Algorithms in image segmentation are performed on image intensity values based on two properties [4]. The first property

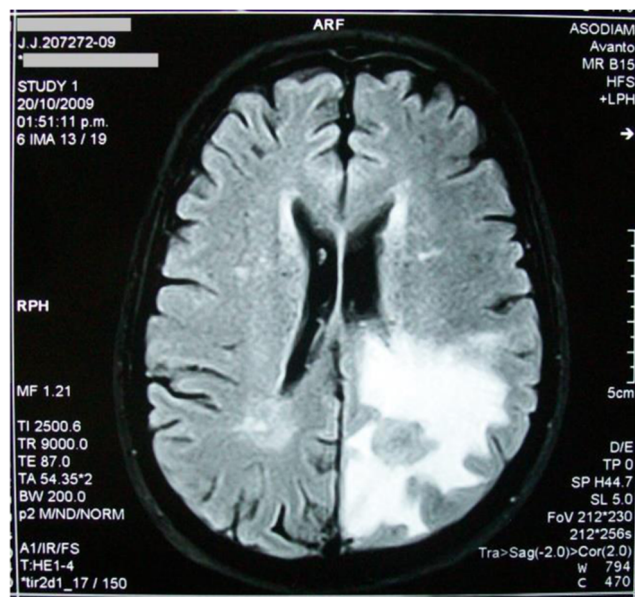


Fig. 1 Brain tumor MRI

is discontinuity, for partitioning the processed image based on intensity changes such as edges and corners. The second property is based on partitioning an image into regions that are similar to groups of predefined criteria. The existing methods are performed on various segmentation processes, but they have some limitations [5–7].

The selection [33] of an appropriate scheme for segmenting a specific image is difficult. In the image processing and computer vision fields, it remains a challenging problem [9]. In this paper, the proposed scheme focuses on efficient preprocessing and feature extraction. A fuzzy logic with spiking neuron model (FL-SNM) is proposed for efficient brain tumor segmentation in MR images [10]. Preprocessing occurs through a modified Kuan filter, to reduce Gaussian and Poisson noise, and edges are preserved by employing an anisotropic diffusion filter. The preprocessed image is then extracted using FLDA to obtain the relevant features. The extracted image is forwarded to FL-SNM as an input, to segment the tumor and non-tumor regions, and FL-SNM is optimized with a CSI algorithm to improve the segmentation accuracy.

## Related work

Many researchers have studied brain tumor segmentation by implementing various methods, but these methods still, face certain limitations. In this section, existing techniques [34] and limitations are surveyed. Hiralal and Menon [11] made a general survey of various segmentation schemes in MRI brain pictures. Si et al. [12] suggested an entropy maximization (EM) - based segmentation approach using a grammatical swarm algorithm for lesion detection in brain MR images. Elsayad [13] proposed back-propagation (BP) and learning vector quantization (LVQ) neural networks to segment the brain MR images into different objects. The BP algorithm was used to train the MRI algorithm. Similarly, the LVQ neural network is also used to classify the different objects in MR images.

Dahshan et al. [14] proposed a hybrid PCA-FFNN-based machine learning [15] technique where principal component analysis (PCA) was used, which decreased the wavelet features. A feed-forward multilayer neural network (FFNN) has been used for automatic detection of brain tumors. Ortiz et al. [16] proposed a self-organizing map (SOM) with a genetic algorithm (GA), two unsupervised neural schemes for brain MR image segmentation. Initially, the histogram scheme was used to segment the whole volume via SOM [35]. Then, GA was used to extract the features. Finally, the segmented regions were classified using SOM with the entropy gradient clustering method [8].

Dong et al. [17] proposed a new classification scheme for back-propagation neural networks (BPNNs) in MRI for

classifying normal or abnormal tumors. Initially, discrete wavelet transform (DWT) - based features are extracted and then some particular features are selected using PCA. Finally, the BPNN is trained using the scaled conjugate gradient (SCG) method, to categorize the MR images.

Liu et al. [18] proposed a self-organizing active contour (SOAC) model. For single-mode MR images, the segmentation task cannot be successfully achieved. Sharma and Mukharjee proposed [19] an artificial neural network fuzzy inference system, with important features selected using a genetic algorithm (GA). After that, fuzzy rules and membership functions are defined based on these, and features are obtained for segmenting brain tumors from MR images.

Logeswari and Karnan [20] proposed hierarchical self-organizing map (HSOM) - based brain MRI segmentation. Results showed better performance, but the method has difficulty in mapping. Pereira et al. [21] suggested a convolutional neural network (CNN)-based segmentation scheme for efficient MRI brain tumor segmentation. Simulation results illustrated the achievement of high performance, with a Dice similarity coefficient measurement of 0.78. However, this scheme takes a long time to train the data and needs large training data sets, so the computational cost is high. Havaei et al. [22] proposed a deep neural networks (DNNs)-based segmentation scheme for MRI. This method shows better performance with respect to accuracy and speed but also has computational complexity.

From the literature survey, it is evident that, tumor diagnosis is very difficult, sensitive task. Very little attention was paid to reduce the high mortality rate of brain tumor. Real time diagnosis of tumor using more reliable algorithms has been the major focus in the latest developments for the detection of brain tumor in MRI has to be improved. Nevertheless, the accuracy and processing time are considered to be major limitations. To solve the above problems, the proposed system focuses on fuzzy logic with SNM. In this automatic segmentation process, FL-SNM has been used for improving efficiency and simplicity.

## Proposed methodology

In recent years the high mortality rate from brain tumors has greatly increased the significance of brain tumor detection. In this paper, the major focus is on real-time diagnosis of tumors using reliable algorithms for detection of a brain tumor with MRI. In this section, the proposed FL-SNM-based brain tumor segmentation is presented. Automatic image processing techniques are implemented for effective detection of tumor

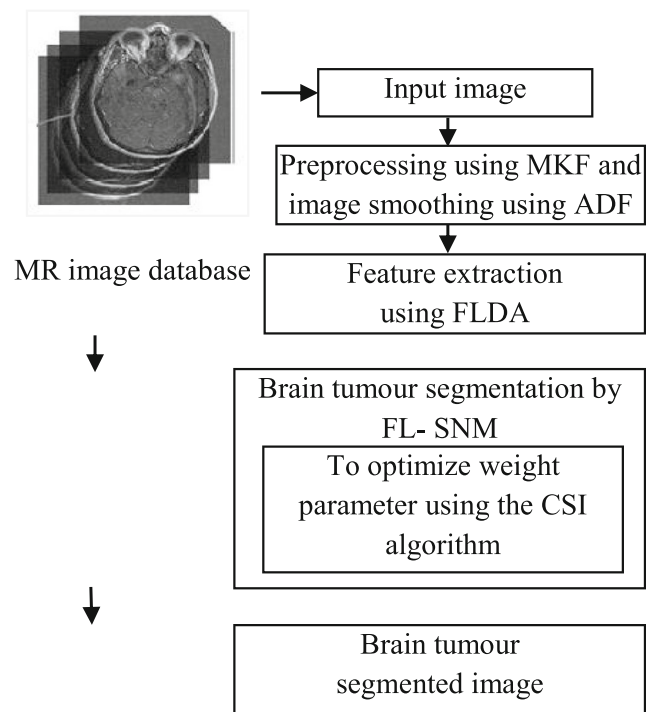


Fig. 2 Overall architecture of proposed FL-SNM scheme

segmentation. The process for the proposed scheme is described in the following subsections. The proposed system flow is presented in Fig. 2.

## System overview

The existing HSOM leads to inaccuracy in training the data because of the network sizes. It uses different layers to train the data and inappropriate methods of choosing the learning parameters for each layer. CNN gives better results, but it fails to give high accuracy due to the network's weights at different scales, and it is quite slow in training the data. In addition, there may be overfitting issues, depending upon the given input data. For this reason, the segmentation results will be inaccurate. To overcome this, the automated FL-SNM is developed for efficient segmentation.

Figure 2 shows the overall architecture of the proposed FL-SNM-based brain tumor segmentation method. The MRI data set was collected from the publicly available website <http://www.medinfo.cs.ucy.ac.cy/index.php/downloads/datasets>. The input data sets contain noise and unwanted data which are subjected to image processing techniques such as preprocessing, feature extraction and segmentation, for improving image contrast and visual quality.

Initially, the input images are preprocessed using MKF, where the minimum MSE of image pixels is selected by

RSA, to improve the PSNR of the image and reduce the MSE. Then, ADF is used, to reduce salt-and-pepper noise to improve the image quality. Subsequently, the required features are extracted using FLDA to reduce the processing time. Afterwards, extracted features are segmented through FL-SNM by training and testing the images, and the parameters are optimized using a CSI algorithm to enhance the segmentation accuracy.

### Preprocessing

Initially, the input image is collected and then resized. Preprocessing is mainly employed to improve the image quality and to reduce noise. Generally, brain images remain clearer, than other medical images, with minimum noise and high quality. The modified Kuan filter is implemented for reducing noise and improving quality.

A Kuan filter is selected due to its high accuracy and the fact that it does not make an approximation to the noise variance within the filter window. It simplifies the multiplicative model of Gauss and Poisson into an additive linear form, but it depends on the effective number of looks (ENL) from an image to decide on a weighting function  $W$ . Therefore, the MKF uses RSA to optimize the weight value in the Kuan filter.

**Denosing step** MRI images usually contain Gaussian and Poisson noise. The modified Kuan filter is utilized to remove noise without eliminating edges or features in the images. However, the noise is transformed from multiplicative noise into a dependent additive noise model. After that, the minimum mean-square error (MSE) condition is applied for estimating the original form of the image, which is given as

$$GL_{i,j} = \sum_{i=1}^{m=3,n=3} \sum_{j=1}^{m=3,n=3} Cp_{i,j} * W_{i,j} + M_{i,j} * (1 - W_{i,j}) \quad (1)$$

where  $(i, j)$  represents the image pixels and  $(m,n)$  represents the rows and columns of the pixel data.  $Cp_{i,j}$  is defined as the center pixel in the filter window  $M_{i,j}$ , which refers to the mean value of intensity within the window and  $W_{i,j}$  is a weighting factor. Depending on the weight, noise reduction is performed and optimized by a random search algorithm (RSA).

A general RSA is described by a sequence of iterates  $\{W_k\}$ ,  $k = 0, 1, \dots, k$ , which depends on the preceding pixel points and the algorithmic parameter  $\Theta$ , comprising the mean vector and the covariance matrix. The current iterates  $W_k$  represent a collection of points. In addition, the iterations are capitalized to denote that they are random variables, reflecting the probabilistic nature of the RSA. It depends on two basic processes: creating candidate points and updating the procedure. The pseudocode of the RSA is given below.

### Algorithm: RSA for weight optimization

Initialize parameters such as dimension (dim), population size (popsize), function target (ftarget) and number of iterations (numIter)

```

for i=1:numIter
    candidate=(rand/10);
    [Wei ww]=weight(I,candidate,numIter);
// I-image
    best=min(ww);
    if best <= ftarget
        break;
    end
end
disp(best);
end
check the condition of iteration and
if satisfied then displayxcap=ybar+(cc*(y1-
ybar))/(cc+((ybar^2+cc)/ENL));
// ybar=rand, cc=mat, ENL=rand
display xcap
else
mat, (i.e., matrix)=N// N- number of pixels
xcap=ybar+(cc*(y1-
ybar))/(cc+((ybar^2+cc)/ENL))
// ybar=mean(mean(mat)), ENL=(ybar/ystad)^2,
cc=((ENL*(ystad)^2)-(ybar)^2)/(ENL+1),
ystad=std2(mat)
display xcap
end
    
```

### Anisotropic diffusion filter

Anisotropic diffusion filters (ADFs) are used [23] mainly to smooth the image and remove noise from digital images without blurring edge. The existing diffusion filters have certain limitations, such as the fact that relevant information may not be accurately characterized and the over filtering issue may occur, during the diffusion process, which is due to the loss of original information [24]. The ADF is used to retain the relevant information during the filtering process.

It includes a selective diffusion mechanism by means of probabilistic characterization of MR images. It processes the regions during the diffusion via the reduction of presumably appropriate information (regions and for diagnosis).

ADF can be defined as

$$\frac{\partial I}{\partial t} = \text{div}[C(|\nabla I|). \nabla I], I(t = 0) = I_0 \quad (2)$$

where  $\nabla$  is the gradient operator,  $\text{div} ( )$  is the divergence operator,  $| \cdot |$  is defined as the magnitude and  $I_0$  represents the initial image. The diffusion coefficient  $C$  is given by

$$C = \frac{1}{\ln\left[e + \left(\frac{\sqrt{L}}{k}\right)^2\right]} \tag{3}$$

where Euler’s value  $e = 2.71828$  and,  $k$  represents the edge magnitude parameter. The filtering scheme benefit is in smoothing small discontinuities, which is initiated through background noise using gradient information. In addition, it can protect large intensity variations caused by edges.

### Feature extraction using FLDA

Fisher’s LDA is used to extract the relevant features for segmentation. Linear discriminant analysis (LDA) has limitations for a singularity problem (it fails when all scattering matrices are singular) and it only extracts features less than one number of classes. It is solved by improving LDA to FLDA through a linear mixture model [25] for attaining a high accuracy rate.

It aims to solve the illumination difficulty by maximizing the ratio of between-class scatter to within-class scatter. It is impossible to find an optimum method of projection with simultaneous separation of multiple tumor classes. It can remove redundant information and retain useful data with minimum storage space and a fast computing speed.

Furthermore, it can reduce the distances between samples in the same class (label), as well as increasing the distances between different classes. It is mainly used to reduce the misclassification error rather than the distance between samples. Consider  $D$ -dimensional samples  $x = \{x_1, \dots, x_m\}$  with a total of  $c$  classes. Their scatter matrix within the class can be defined as shown in eq. (4).

$$S_W = \frac{1}{N} \sum_{i=1}^c \sum_{x_{ij} \in c_i} \frac{1}{N} (x_{ij} - m_i)(x_{ij} - m_i)^T \tag{4}$$

where  $m_i = \sum_{x_{ij} \in c_i} \frac{1}{N_i} x_{ij}$ ,  $N_i$  are data points for class  $i$  and the scatter matrix between classes is given as

$$S_B = \sum_{i=1}^c \frac{N_i}{N} (m_i - \mu)(m_i - \mu)^T \tag{5}$$

$$\text{where } \mu = \frac{1}{N} \sum_{j=1}^c \sum_{k=1}^{N_j} j_k.$$

The total scatter matrix and the final function can be defined as

$$S_T = S_W + S_B \tag{6}$$

$$S_T = \frac{1}{N} \sum_{j=1}^c \sum_{k=1}^{N_j} (x_{ij} - \mu)(x_{ij} - \mu)^T \tag{7}$$

To minimize the misclassification error and maximize the Raleigh quotient, the below equation is used. It is equivalent to solving the following generalized eigenvalue problem.

$$J(Z) = \frac{Z^T S_B Z}{Z^T S_W Z} \text{ Over } Z \tag{8}$$

$$S_B v_i = \lambda_i S_W v_i \tag{9}$$

where,  $\lambda_i$  is the observed variance when data are projected on  $v_i$  and  $v_i$  is the corresponding eigen-vector for class  $i$ , defined as eigen-vector or the  $i^{\text{th}}$  Fisher’s linear discriminant. The rank of  $S_B$  will be the full rank. It has more features than the number of classes [36] based on the technique and the linear mixture problem can be resolved.

The gray-level co-occurrence matrix (GLCM) based on statistical features [6] is extracted. In total, 24 features [26] can be extracted, but only seven features are considered for efficient classification. These are: homogeneity (H) measures image homogeneity as it assumes larger values for smaller gray tone differences in pair elements. It has maximum value when all elements in the image are same; contrast (C) represents the difference between the highest and the lowest values of a contiguous set of pixels, energy (E) which detects the disorders in textures and reaches a maximum value equal to one. Variance (V) is a measure of heterogeneity. It increases when the gray level values differ from their mean. Correlation (Co) is a measure of gray tone linear dependencies in the image; entropy (En) measures the disorder or complexity of an image; complex textures have strong entropy; and mean (M). By, extracting these features only, processing time is decreased.

### Tumor segmentation using FL-SNM

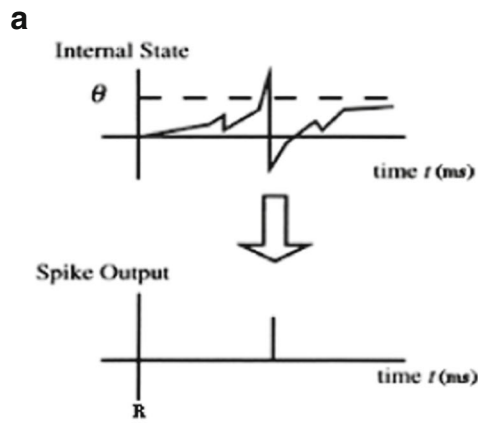
SNM is utilized for detecting the tumor region from the MR image. SNM is composed of fuzzy logic input values in order to develop a user-friendly system. Generally, a Hebbian learning [27] process is carried out for the functions among the spiking neurons. If two neurons on either side of a synapse are activated simultaneously, then the strength of that synapse is selectively increased [28]. The model input state (spikes) and their membership function (Gaussian) are based on external inputs, as shown in Figs. 3a and b [29].

The whole process of the proposed FL-SNM is shown in Fig. 4. Here, the image pixels based on seven features are considered as spiking inputs and their fuzzy rules are generated using the formula given below.

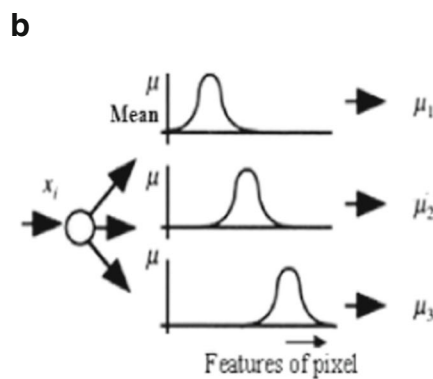
$$\mu_{A_{i,j}}(x_j) = \exp\left(-\frac{(x_j - a_{i,j})^2}{b_{i,j}}\right) \tag{10}$$

$$y_i = \prod_{j=1}^m v_{i,j} \cdot \mu_{A_{i,j}}(x_j) \tag{11}$$

where  $\mu$  is the membership function,  $x_j$  is defined as the internal state variable,  $A_{i,j}$  and  $v_{i,j}$  represent the part of  $j^{\text{th}}$  input for the estimation of the  $i^{\text{th}}$  image pixel feature state,  $a_{i,j}$  is defined as the middle value,  $b_{i,j}$  represents the width of the



Spiking (Pixel) Neuron Model



Membership Function-Based External Inputs

**Fig. 3** **a** Spiking (Pixel) neuron model. **b** Membership function - based external inputs

membership function,  $y_i$  denotes the product of fuzzy inference and can be considered as an input to the spiking neurons and  $m$  denotes the total number of inputs.

A sample of fuzzy if-then rules framed for the MRI brain tumor classification is given below.

- Rule 1: If  $x$  is  $C1$  and  $y$  is  $H1$  and  $z$  is  $E1$  and  $u$  is  $M1$  and  $w$  is  $En1$  and  $a$  is  $Co1$  and  $b$  is  $V1$ , then output = 1
- Rule2: If  $x$  is  $C2$  and  $y$  is  $H2$  and  $z$  is  $E2$  and  $u$  is  $M2$  and  $w$  is  $En2$  and  $a$  is  $Co2$  and  $b$  is  $V2$ , then output = 2
- Rule3: If  $x$  is  $C3$  and  $y$  is  $H3$  and  $z$  is  $E3$  and  $u$  is  $M3$  and  $w$  is  $En3$  and  $a$  is  $Co3$  and  $b$  is  $V3$ , then output = 3 (where, the variables represents homogeneity (H), contrast (C), energy (E), mean (M), variance (V), correlation (Co) and entropy (En))

The above rules form the input for the FL-SNM architecture to identify the region affected by a tumor. In the affected region, the region space is segmented; otherwise, it will show that it is not affected by any tumor. Based on the fuzzy rules, the following predictions can be made.

The initial state  $hn_i(t)$  of the  $i^{th}$  spiking neuron (pixel value) is defined as a membrane potential at the discrete time  $t$ :

$$hn_i(t) = \tanh(hn_i^{syn}(t) + hn_i^{ext}(t) + hn_i^{ref}(t)) \quad (12)$$

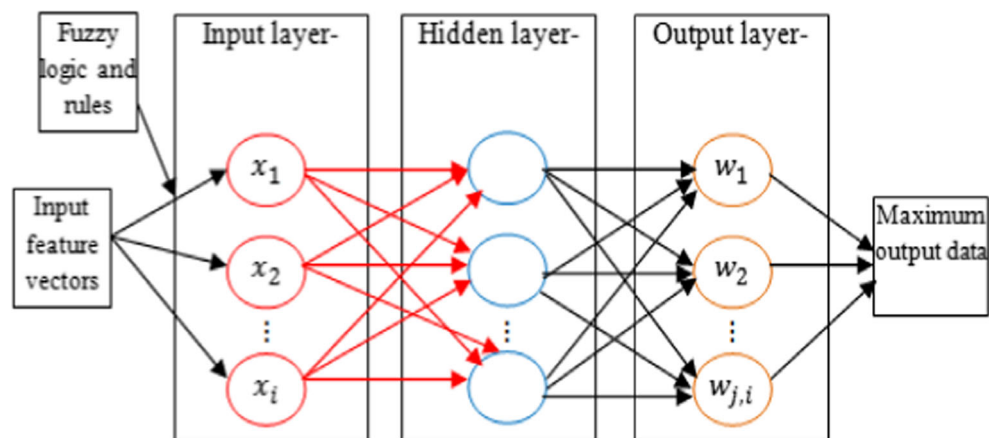
where  $hn_i^{ext}(t)$  represents the external environment input influences on the  $i^{th}$  neuron,  $hn_i^{syn}(t)$  represents the incorporation of the pulses, (i.e., pixel features) from the other fully connected neuron (pixel) outputs and  $hn_i^{ref}(t)$  defines the refractoriness of the neuron. The tan function is used to avoid bursts of neuronal firings.

$$hn_i^{ext}(t) = \prod_{j=1}^m v_{i,j} \cdot \exp\left(-\frac{(x_j - a_{i,j})^2}{b_{i,j}}\right) \quad (13)$$

$$hn_i^{syn}(t) = \gamma^{syn} \cdot hn_i(t-1) + \sum_{j=1, j \neq i}^n w_{j,i} \cdot hn_j^{PSP}(t-1) \quad (14)$$

where  $\gamma^{syn}$  represents a temporal discount rate and PSP represents a post-synaptic potential, adopted by the synaptic weight  $w_{j,i}$  to obtain the effectual PSP. When the internal state

**Fig. 4** General structure of FL-SNM for brain tumor segmentation



of the  $i^{th}$  neuron reaches a predefined threshold level  $\theta = 4.9664$ , this threshold is cached from the CSI, and the pulse output is defined as

$$O_i(t) = \begin{cases} 1 & \text{if } hn_i(t) \geq \theta \\ 0 & \text{otherwise} \end{cases} \quad (15)$$

where  $\theta$  is defined as the threshold for firing. When the neuron is fired, the total firing rate ( $R$ ) is subtracted from the  $hn_i^{ref}(t)$  value of neuron  $i$ , defined as follows:

$$hn_i^{ref}(t) = \begin{cases} \gamma^{ref} \cdot hn_i^{ref}(t-1) - R & \text{if } O_i(t-1) = 1 \\ \gamma^{ref} \cdot hn_i^{ref}(t-1) & \text{otherwise} \end{cases} \quad (16)$$

where  $\gamma^{ref}$  is defined as a discount rate of  $hn_i^{ref}$  and  $R > 0$ . The pre-synaptic spike output is transmitted to the connected neuron by the weight connection.

The PSP is calculated as

$$hn_i^{PSP}(t) = \begin{cases} 1 & \text{if } O_i(t) = 1 \\ \gamma^{PSP} \cdot hn_i^{PSP}(t-1) & \text{otherwise} \end{cases} \quad (17)$$

where  $\gamma^{PSP}$  is defined as the discount rate of  $hn_i^{PSP}$ . Generally, weights between neurons are modified by Hebbian learning. However, this is only applied when the following condition is satisfied:

$$\text{if } 0 < n_i^{PSP}(t-1) < n_i^{PSP}(t) \quad (18)$$

When this condition is satisfied, the weight parameter  $w_{j,i}$  is trained based on the Hebbian learning rule [6] defined as

$$w_{j,i} \leftarrow \left( \gamma^{wt} w_{j,i} + \frac{\xi^{wt} n_i^{PSP}(t-1)}{n_i^{PSP}(t)} \right) \quad (19)$$

where  $\gamma^{wt}$  is defined as the discount rate of the learning rate  $\xi^{wt}$ . This dynamically updates the weight values. For accurate weight value prediction, an optimization [30] algorithm such as chicken behavior-based swarm intelligence (CSI) is used to improve the segmentation accuracy.

This has a high convergence rate and gives better weight values, improving the segmentation accuracy. The general structure of FL-SNM for brain tumor segmentation is shown in Fig. 4.

### Chicken behavior-based swarm intelligence (CSI) for weight optimization

The swarm intelligence system is an artificial intelligence algorithm based on the natural behavior of swarms or agents. It is robust due to the simple design and is also flexible with high a processing speed.

### Basic working principle for CSI

The algorithm was developed by Meng et al. [31], based on the natural behavior of chickens. Here, for roosters ( $R_N$ ), hens ( $H_N$ ), chicks ( $C_N$ ) and mother hens ( $M_N$ ), basic food search behavior has been considered to search for the optimal result.  $N$ -is the total number of chickens.

- **Step 1:** The initial position of all chickens is  $x_{i,j}(t) (i \in [1, \dots, N], j \in [1, \dots, D])$ , where  $D$  is the dimensionality of the search space at time  $t$  for each chicken. Roosters can be considered as best fits because they can easily detect their food, whereas the hens and chicks search for their food.

Therefore, the rooster's  $R_N$  position update is defined as

$$x_{i,j}^{(t+1)} = x_{i,j}(t) (1 + randn(0, \sigma^2)), \quad (20)$$

$$\sigma^2 = \begin{cases} 1, & f_i \geq f_k, k \in [1, N], k \neq i \\ \exp\left(\frac{f_k - f_i}{|f_i| + \varepsilon}\right), & \text{otherwise} \end{cases}$$

where  $randn(0, \sigma^2)$  represents a Gaussian distribution with standard deviation  $\sigma$  and mean 0,  $\varepsilon$  is defined as a small constant to avoid the zero-division-error,  $k$  represents the rooster's index and is randomly chosen from the rooster group ( $k \neq i$ ) and  $f_i$  represents the fitness rate of particle  $i$ .

- **Step 2:** following the roosters, the hens search for their food and the hens'  $H_N$  position update equations can be defined as

$$x_{i,j}^{t+1} = x_{i,j}^t + C_1 rand(x_{r1,j}^t - x_{i,j}^t) + C_2 rand(x_{r2,j}^t - x_{i,j}^t) \quad (21)$$

$$C_1 = \exp((f_i - f_{r1}) / (|f_i| + \varepsilon)) \quad (22)$$

$$C_2 = \exp(f_{r2} - f_i) \quad (23)$$

The chicks search for their food based on the hens' food search and the chicks' position update equations can be defined as eqs. (22) and (23). Finally, the one with best fitness is updated:

$$x_{i,j}^{t+1} = x_{i,j}^t + F(x_{m,j}^t - x_{i,j}^t) \quad (24)$$

where  $x_{m,j}^t$  is the hen or mother hen position and  $F \in [0, 2]$  is defined as the coefficient. Based on the above fitness evaluation, the optimal weight is predicted and is used in the effective training and testing for tumor segmentation.

### CSI for optimal weight selection

- **Step 1:** an initial generation of chickens (features) is formed randomly with a limited search space. Each

chicken swarm is defined as a weight vector (W) of all control variables.

- **Step 2:** the best values of all chicken solutions are calculated by running the feature vectors.

The control variable values are taken for various roosters and incorporated in the system feature vector and the weight is run.

Then, the total weight of each chicken is calculated.

- **Step 3:** the best hen’s food search is determined, which is denoted as the global best-fitness value.

Based on the food search mechanism, the search results for the rooster, hen and chicks are arranged in ascending order, based on their sound echoes.

The first hen will be the candidate with the best food searching, (i.e., best weight value) giving the best global index value.

- **Step 4:** a new rooster is generated around the global best swarm by adding or subtracting a normal random number. It should be ensured that the control variables are within their limits.
- **Step 5:** rooster, hen, and chicks are compared to find the one with the best global fitness value. This process takes place over a number of iterations.

Steps 2–4 are replicated until the stopping criterion has been achieved.

### Measuring segmentation

The performance metrics for FL-SNM, based on the brain tumor segmentation method, are estimated. Measures such as sensitivity (Se), specificity (Sp), accuracy (Ac), precision (Pr), recall (Re), F-measure, geometrical mean (G-mean), and Dice similarity coefficient (DSC) are used.

Let *TP* be the true positive rate of images, *FP* the false positive rate of images, *TN* the true negative rate of images and *FN* the false negative rate of images.

The positive predictive value (PPV) is the probability that the disease is present when the test is positive.

The negative predictive value (NPV) is the probability that the disease is not present when the test is negative.

$$Se = TP / (TP + FN) \tag{25}$$

$$Sp = TN / (TN + FP) \tag{26}$$

$$Ac = (TP + TN) / (TP + FN + TN + FP) \tag{27}$$

$$Pr = TP / (TP + FP) \tag{28}$$

$$Re = TP / (TP + FN) \tag{29}$$

$$F = 2 \cdot \frac{Pr \cdot Re}{Pr + Re} \tag{30}$$

$$\text{Positive Predictive Value (PPV)} = TP / (TP + FP) \tag{31}$$

$$\text{Negative Predictive Value (NPV)} = TN / (TN + FN) \tag{32}$$

$$\text{False Positive Rate (FPR)} = 1 - Sp \tag{33}$$

$$\text{False Negative Rate (FNR)} = 1 - Se \tag{34}$$

$$\text{Dice Similarity Coefficient (DSC)} = \frac{2TP}{FP + 2TP + FN} \tag{35}$$

$$\text{G-mean} = \sqrt{TP\_rate * TN\_rate} \tag{36}$$

### Results and discussion

In this section, the FL-SNM scheme is evaluated and analyzed, together with the existing CNN and HSOM methods. Initially, the MRI database images are trained and tested. In the training process, 10 normal and 10 segmented images are used for the proposed FL-SNM model. The images are selected randomly. Processing time varies from system to system, depending on the processing speed of the processor. The simulation results are estimated using MATLAB R2017a running in Windows 10. Kuan filter, MKF and ADF results are shown in Table 1. This table shows that MKF attained better results than KF, due to the efficient optimization of MKF. In addition, ADF gives better MSE and PSNR results than KF and MKF, due to the efficient image smoothing.

In Table 1, the performances of the presented filtering schemes have been measured in terms of MSE, PSNR and weight values for input image 1.

From the observations, MKF attained good PSNR, MSE and weight values compared to KF, with a good optimized result. Therefore, it reduces noise at the rate of 0.0705% compared with KF. After obtaining the preprocessed outcome from MKF, the ADF is used for effective smoothing, which reduces the noise at the rate of 19.339% compared with MKF, as shown in Table 1. Based on the performance measures, the preprocessing results for two images are shown in Fig. 5.

**Table 1** Performance measures for preprocessing

Performance Measures	KF	Proposed MKF	ADF
MSE	31.198	31.176	25.147
PSNR	33.223	33.227	34.16
Weight value	0.0812	0.0747	0.1429

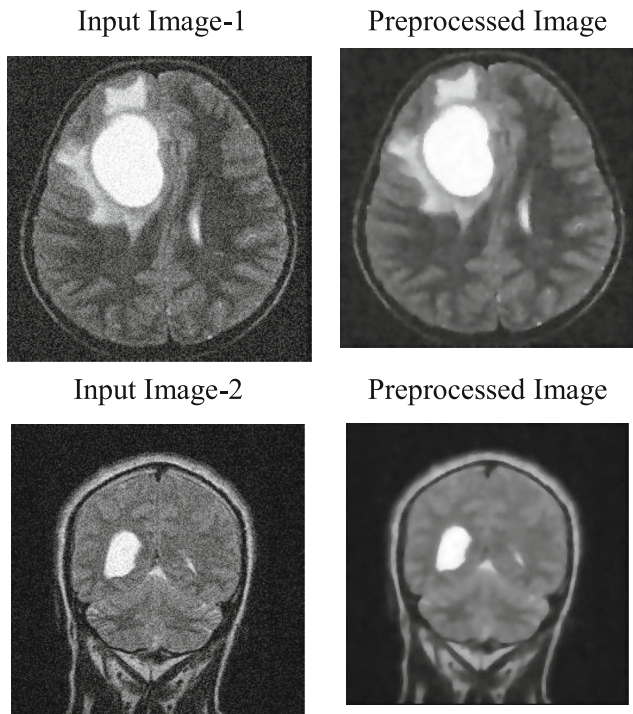


Fig. 5 Preprocessing results for input images

The feature extractions for the two images using FLDA are predicted in Fig. 6.

The feature extraction results are obtained as numerical values. Therefore, the simulation results of feature extraction are same as for the preprocessing image.

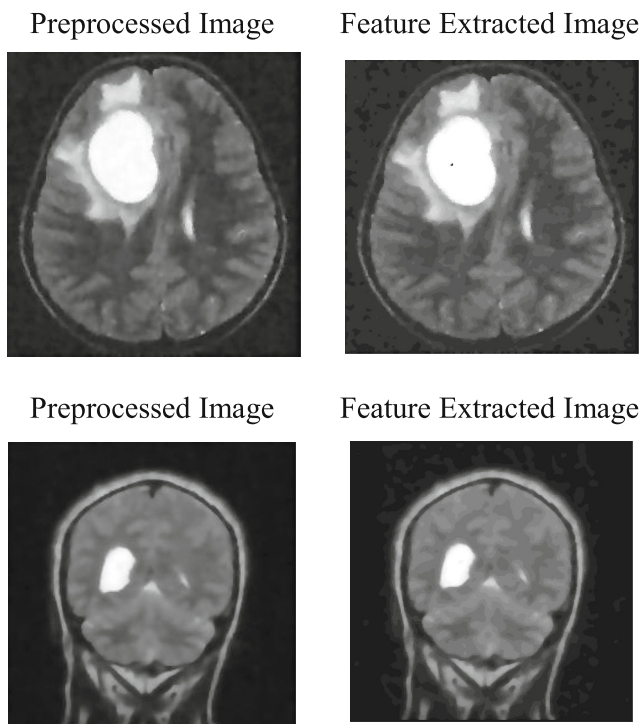


Fig. 6 Feature Extraction results for input images

Table 2 Optimized Weight Values of Proposed Scheme

Number of Iterations	Optimized Weight Values
1	0.9960
2	0.9854
3	0.9748
4	0.9643
5	0.9537
6	0.9431
7	0.9325
8	0.9220
9	0.9114
10	0.9008
11	0.8902
12	0.8797
13	0.8691
14	0.8585
15	0.8479
16	0.8374
17	0.8268
18	0.8162
19	0.8056
20	0.7950

The gray-level co-occurrence matrix (GLCM) based on statistical features, is extracted. The extracted feature values of input image 1 were predicted as: contrast:  $1.3787e-04$ , correlation: 0, energy: 1.0000, homogeneity: 1.0000, mean: 68.7232, variance:  $3.0146e+03$  and entropy:  $2.6615e-04$ . The optimized weight value of input image 1 has been predicted from CSI and is shown in Table 2. This shows sample numbers of iterations and their corresponding weight values. The condition gets satisfied and the final optimized value of this Scheme 0.2768 is obtained.

Finally, the tumor region is predicted in this layer. Based on these values, the input image is tested and the final segmented results are displayed. For example, the two input images have been tested and their segmented results are shown in Fig. 7. This figure illustrates the tumor segmented region in an efficient manner for the proposed FL-SNM scheme.

The proposed FL-SNM scheme evaluates the eight volume metric results for brain MR images and their numerically evaluated values are predicted as shown in Table 3. This shows the performance variations in FL-SNM when the number of input images is increased from two to ten. Here, ten images are considered for the testing process. The overall average values of all performance measures are predicted in this table. The average performance value of FL-SNM is: accuracy 94.87%, sensitivity 92.07%,

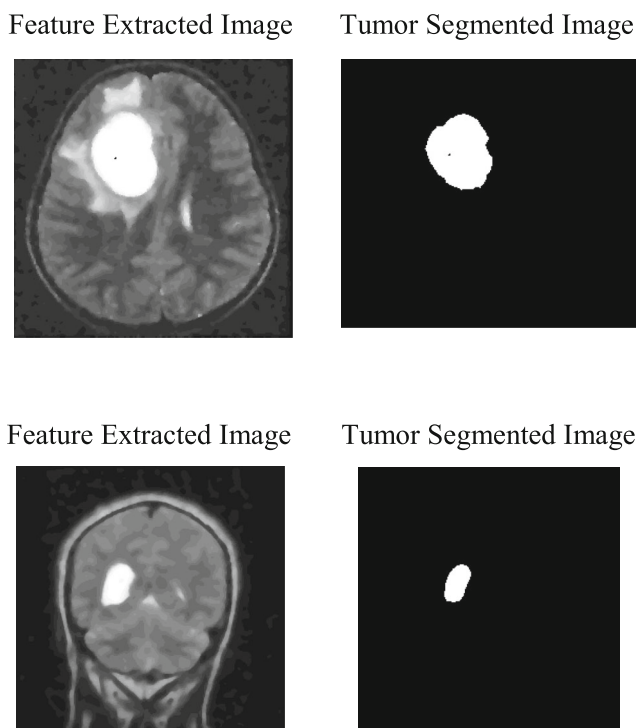


Fig. 7 Tumor segmentation results for input images

specificity 99.34%, precision 89.36%, recall rate 88.39%, F-measure 95.06%, G-mean 95.63% and DSC rate 91.20%. These performance results are compared with existing schemes and their numerical results are shown in Table 3.

The proposed FL-SNM brain tumor segmentation attained high accuracy due to efficient optimization with an effective feature extraction process. Figures 8, 9 and 10 show the overall performance comparison for the proposed FL-SNM and the existing CNN and HSOM brain tumor segmentation schemes. They demonstrate that the accuracy value is high in the proposed FL-SNM scheme, owing to optimal weight prediction with efficient feature extraction, which reduces the processing time and also improves the

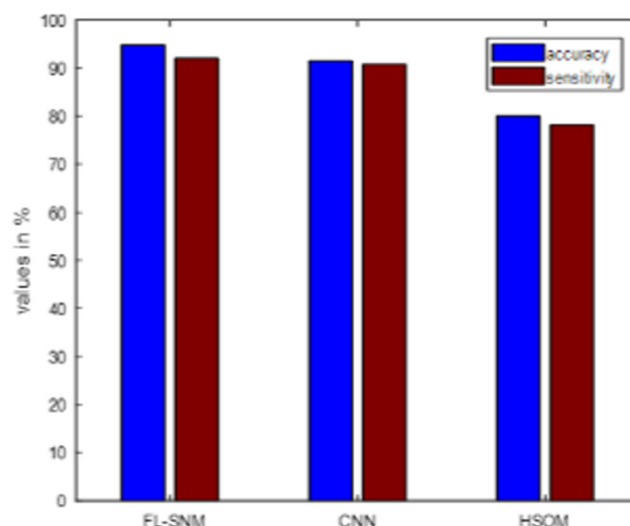


Fig. 8 Accuracy and sensitivity performance comparison for tumor segmentation schemes

quality of the image. For the above reasons, the results of the FL-SNM scheme are improved.

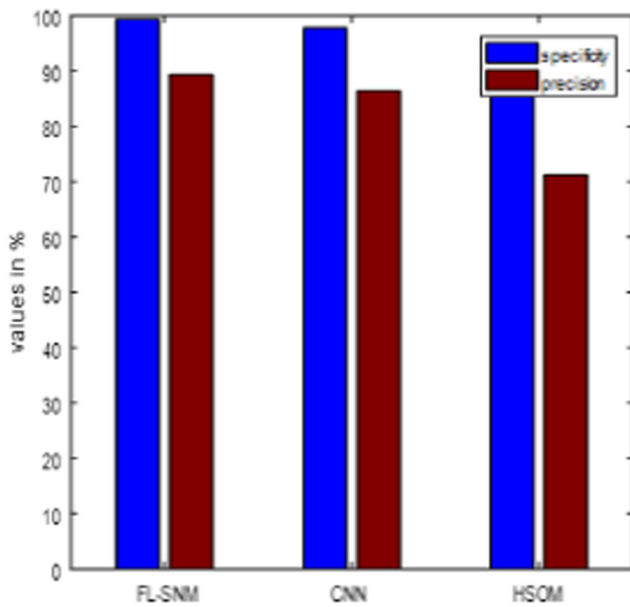
Figure 8 shows that the accuracy of FL-SNM is 3.37% and 14.77% higher than CNN and HSOM. The sensitivity of FL-SNM is 1.27% higher than CNN and 13.87% higher than the HSOM scheme. Due to the effective noise reduction and the retrieval of useful information [32] using filtering techniques, the FL-SNM scheme attained improved results.

Figure 9 shows that the specificity of FL-SNM is 1.62% and 13.94% higher than CNN and HSOM. The precision of FL-SNM is 2.95% and 18.22% higher than the CNN and HSOM schemes. Due to high TP and TN results, the specificity and precision of FL-SNM is increased.

Figure 10 shows that the F-measure of FL-SNM is 7.52% and 16.81% higher than CNN and HSOM. The G-mean of FL-SNM is 8.18% and 17.16% higher than the CNN and HSOM schemes. The recall value is increased by 2.92% and 16.05% compared with CNN and HSOM respectively. Due to the high precision and recall

Table 3 Performance evaluation value for proposed FL-SNM

Input Images	Accuracy- Ac (%)	Sensitivity- Se (%)	Specificity - Sp (%)	Precision - Pr (%)	Recall - Re (%)	F-measure (%)	G-mean (%)	DSC (%)
2	95.45	92.8	99	88.13	88.40	94.30	94.65	90.68
4	95.1	92.1	100	89.1	87.90	95.30	95.65	90.97
6	95.13	92.9	100	92.12	88.21	96.47	96.74	91.26
8	94.45	91.2	98.9	88.34	88.87	95.05	95.98	91.42
10	94.23	91.34	98.8	89.13	88.56	94.16	95.12	91.67
AVG	94.87	92.07	99.34	89.36	88.39	95.06	95.63	91.20



**Fig. 9** Specificity and precision performance comparison for tumor segmentation schemes

value, the F-measure and G-mean of FL-SNM are increased. In addition, it shows the Dice similarity coefficient (DSC) performance results for all algorithms. It shows illustrates that the proposed FL-SNM has attained a higher DSC value by 2.42% and 7.57% compared to the existing CNN and HSOM, due to high TP and low FP.

The performance of the proposed FL-SNM and the existing segmentation schemes CNN and HSOM, are evaluated in terms of PPV, FPR, NPV, and FNR, and their numerical outcomes are evaluated. Table 4 shows that,

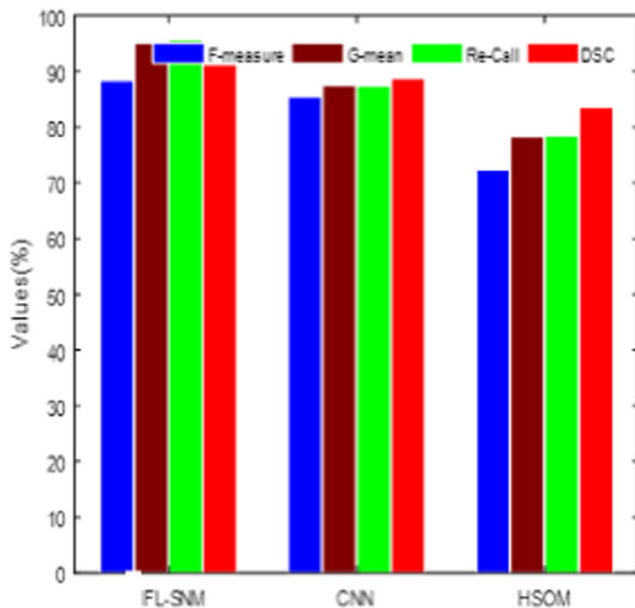


**Fig. 10** F-measure, G-mean, Recall and DSC performance comparison for tumor segmentation scheme

**Table 4** Numerical results of other parameters for all segmentation schemes

Segmentation Scheme	PPV (%)	NPV (%)	FPR (%)	FNR (%)
FL-SNM	0.924	0.814	0.2080	0.1970
CNN	0.8822	0.8939	0.1000	0.0800
HSOM	0.9221	0.9174	0.0600	0.0762

the proposed FL-SNM has achieved the best results compared with existing CNN and HSOM schemes. Because FL-SNM requires less training time, the speed of the process is increased. The processing data set values have been improved based on the fast process. Here, the true positive and negative results are predicted correctly using SNM, and it increases the accuracy of segmentation.

Table 5 shows that the CNN method has only attained a sensitivity of 90.8%. However, it has a lower specificity than the FL-SNM scheme, due to its high computational complexity. The HSOM also achieved less accuracy than the proposed FL-SNM scheme, due to its high computation time.

A graphical representation of all segmentation schemes is shown in Fig. 11. This shows that the proposed FL-SNM achieved good performance in terms of high accuracy (94.87%), sensitivity (92.07%), specificity (99.34%), precision (89.36%), recall (88.39%), F-measure (95.06%), G-mean (95.63%), and DSC (91.2%), compared with existing CNN and HSOM schemes. Table 5 shows the numerical evaluations for the overall performance matrices. The proposed FL-SNM results are high compared with the existing CNN and HSOM methods. When the number of images increases, the numerical evaluation results of the proposed FL-SNM also increase, because FL-SNM takes less processing time and has efficient feature extraction.

**Table 5** Numerical values of overall performance for all segmentation methods

Performance Matrices	Proposed FL-SNM (%)	CNN (%)	HSOM (%)
Accuracy-Ac	94.87	91.5	80.1
Sensitivity-Se	92.07	90.8	78.2
Specificity-Sp	99.34	97.72	85.4
Precision-Pr	89.36	86.41	71.14
Recall-Re	88.39	85.47	72.34
F-measure	95.06	87.54	78.25
G-mean	95.63	87.45	78.47
DSC	91.2	88.78	83.63

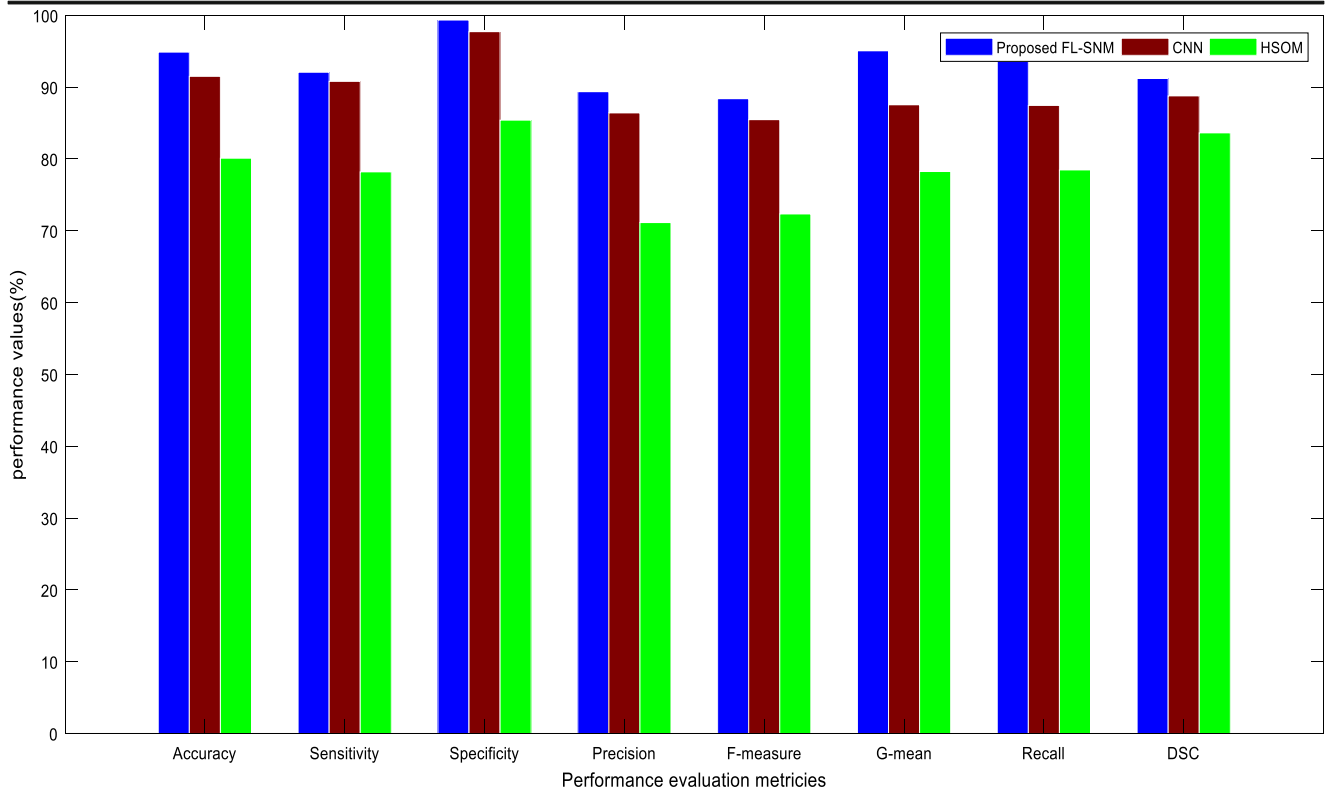


Fig. 11 Performance metrics for brain tumor segmentation schemes

Figure 12 shows a graphical representation of the processing time performance comparison for the proposed FL-SNM and the existing CNN and HSOM segmentation schemes. It illustrates that the proposed FL-SNM took less processing time of (2.70 s) than CNN (3.17 s) and HSOM (3.64 s), due to the efficient feature extraction and CSI optimization.

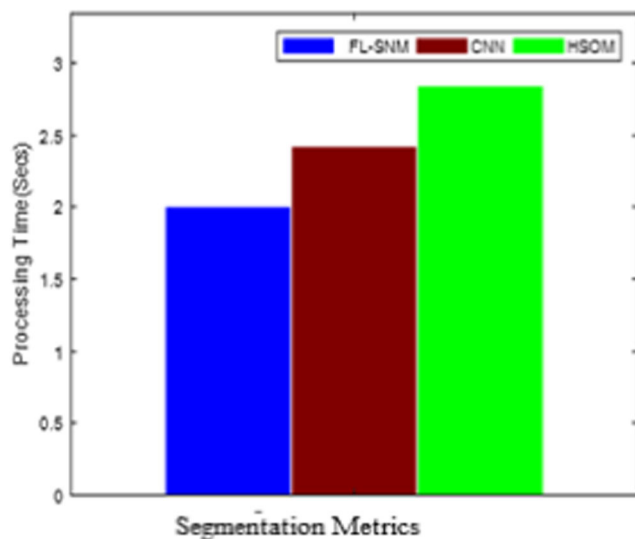


Fig. 12 Processing time comparison for all brain tumor segmentation schemes

### Conclusion

FL-SNM-based brain tumor segmentation has been proposed in this work, with an optimization scheme for increasing segmentation accuracy. The main purpose of this segmentation scheme is to extract the brain tumor portion in an efficient manner and to classify the tumor and non-tumor regions. Initially, the input MR image undergoes preprocessing and feature extraction to extract the relevant features of the tumor region. The FL-SNM with CSI is applied for segmenting the tumor region from the brain image for diagnosis.

The experimental results show the effectiveness of the proposed FL-SNM scheme, which attained high performance in terms of sensitivity, specificity, precision, F-measure, G-mean and accuracy, compared with the existing CNN and HSOM schemes. In addition, its robustness is high.

In the future, this study will be extended for various brain tumor types and for larger data sets. The tumors are recognized based on their shape, size, and changes of tumor growth rate with the same patient. Certain features, such as border, matrix, calcification and texture, will be considered for identifying the tumor types which are used for real-time applications. Optimization, meta-heuristic search algorithms and to recognize more adaptive models with some other neural network or other segmentation schemes will be used for efficient segmentation. This method aids doctors in the early detection of brain tumors, which may help to save lives.

## Compliance with ethical standards

**Conflict of Interest** The authors have no conflict of interest.

**Human and animal rights** This article does not contain any studies with human participants performed by any of the authors

**Ethical approval** This article does not contain any studies with human participants or animals performed by any of the authors

## References

- Dawngliana, M., Deb, D., Handique, M. and Roy, S., Automatic brain tumour segmentation in mri; hybridized multilevel thresholding and level set. *International Symposium on Advanced Computing and Communication*, 219–223, 2015.
- Zabir, I., Paul, S., Rayhan, M. A., Sarker, T., Fattah, S. A., and Shahnaz, C., Automatic brain tumor detection and segmentation from multi-modal MRI images based on region growing and level set evolution. *IEEE International WIE Conference on Electrical and Comput. Eng.*:503–506, 2015.
- Cottet, G.-H., and Ayyadi, M. E. A., Volterra type model for image processing. *IEEE Trans. Image Process.* 7:292–303, 1998.
- Acharya, J., Gadhiya, S., and Raviya, K., Segmentation techniques for image analysis: a review. *Int J ComputSci Manage Res* 2(4): 1218–1221, 2013.
- Naik, D., and Shah, P., A review on image segmentation clustering algorithms. *Int J ComputSci Inform Technol* 5(3):3289–3293, 2014 ISSN: 0975-9646.
- Christe, S. A., Malathy, K., and Kandaswamy, A., Improved hybrid segmentation of brain MRI tissue and tumor using statistical features. *ICTACT J. Image Video Process* 1(1):34–49, 2010.
- Seerha, G. K., and Kaur, R., Review on recent image segmentation techniques. *Int J. ComputSci Eng (IJCSE)* 5(2):109–112, 2013 ISSN: 0975-3397.
- Liu, J. and Guo L., A New Brain MRI Image Segmentation Strategy Based on Wavelet Transform and K-means Clustering. *IEEE International Conference on Signal Pro-cessing, Communications and Computing (ICSPCC)*, 1–4, 2015.
- Dass, R., and Priyanka Devi, S., Image segmentation techniques. *Int J. Electron Commun Technol.* 3(1):66–70, 2012 ISSN: 2230-7109 (Online).
- Amin, S. A. and Megeed, M.A., Brain tumour diagnosis systems based on artificial neural networks and segmentation using MRI. *The 8th International Conference on INFOmatics and systems*, 119–124, 2012.
- Hiralal, R., and Menon, H. P., A survey of brain MRI image segmentation methods and the issues involved. *Advances in Intelligent Systems and Computing* 530:245–259, 2016. [https://doi.org/10.1007/978-3-319-47952-1\\_19](https://doi.org/10.1007/978-3-319-47952-1_19) Springer International Publishing.
- Si, T., De, A., and Bhattacharjee, A. K., Brain MRI segmentation for tumor detection via entropy maximization using Grammatical Swarm. *Int. J. Wavelets Multiresolution Inf. Process.* 13(5):1–8, 2015. <https://doi.org/10.1142/S0219691315500393>.
- Elsayad, A.M., Classification of breast cancer database using learning vector quantization neural networks. *Saudi Association of Health Informatics*, 1–9, 2014; <https://www.researchgate.net/publication/242616752>
- El-Sayed, A., El-Dahshan, E. S. A., Mohsen, H. M., Revett, K., and Salem, A. B. M., Computer-aided diagnosis of human brain tumor through MRI: A survey and a new algorithm. *Expert Syst. Appl.* 41:5526–5545, 2014. <https://doi.org/10.1016/j.eswa.2014.01.021>.
- Hyakin, S., *Neural Networks and Learning Machines*, 3rd Edition. Upper Saddle River: Pearson Prentice Hall, 2011.
- Ortiz, A., Gorriz, J. M., Ramirez, J. and Salas-Gonzalez, D., Unsupervised Neural Techniques Applied to MR Brain Image Segmentation, *Advances in Artificial Neural Systems*. Hindawi Publishing Corporation. 457590:7, 2012. 10.1155/2012/457590.
- Zhang, Y., Dong, Z., Wua, L., and Wang, S., A hybrid method for MRI brain image classification. *Expert Syst. Appl.* 38:10049–10053, 2011. <https://doi.org/10.1016/j.eswa.2011.02.012>.
- Liu, J., Li, M., Wang, J., Wu, F., Liu, T., and Pan, Y. A., Survey of MRI-Based Brain Tumour Segmentation Methods. *Tsinghua Sci. Technol.* 19:578–595, 2014.
- Sharma, M., and Mukharjee, S., Brain tumor segmentation using hybrid genetic algorithm and Artificial Neural Network Fuzzy Inference System (ANFIS). *International Journal of Fuzzy Logic Systems (IJFLS)* 2(4):31–42, 2012. <https://doi.org/10.5121/ijfls.2012.240331>.
- Logeswari, T., and Karman, M., An enhanced implementation of brain tumor detection using segmentation based on soft computing, *IACSIT'10. International Journal of Computer Theory and Engineering* 2(4):1793–8201, 2010 586-590.
- Pereira, S., Pinto, A., Alves, V., and Silva, C. A., Brain tumor segmentation using Convolutional Neural Networks in MRI images. *IEEE Trans. Med. Imaging* 35(5):1240–1251, 2016. <https://doi.org/10.1109/TMI.2016.2538465>.
- Havaei, M., Davy, A., Warde-Farley, D., Biard, A., Courville, A., Bengio, Y., Pal, C., Jodoin, P.-M., and Larochelle, H., Brain tumor segmentation with deep neural networks. *Med. Image Anal.* 35:18–31, 2017. <https://doi.org/10.1016/j.media.2016.05.004>.
- Weickert, J., *Anisotropic Diffusion in Image Processing*. Stuttgart: BG. Teubner, 1998.
- Ramos-Llordén, G., Vegas-Sánchez-Ferrero G, Martín-Fernandez M, Alberola-López C and Aja-Fernández S. Anisotropic diffusion filter with memory based on speckle statistics for ultrasound images. *IEEE Trans. Image Process.* 24(1):345–358, 2015.
- Shimabukuro, Y. E., and Smith, J. A., The least-squares mixing models to generate fraction images derived from remote sensing multispectral data. *IEEE Trans on Geoscience and Remote Sensing* 29(1):16–20, 1991.
- Gerstner, W., and Kistler, W. M., *Spiking neuron models*. Cambridge: Cambridge University Press, 2002.
- Mefthah, B., Lezoray, O., Benyettou, A., Segmentation and Edge Detection Based on Spiking Neural Network Model Neural Process Lett published on august 20, 2010. <https://doi.org/10.1007/s11063-010-9149-6>.
- Hebb, D. O., *The Organization of Behavior*. New York: Wiley and Sons, 1949.
- Mefthah, B., Benyettou, A., Lezoray, O., and Debakla Image, M., Segmentation with Spiking Neuron Network, CP1019, *Intelligent Systems and Automation*, 1st Mediterranean conference. College Park: American Institute of Physics, 2008.
- Zhang, Y., Wang, S., Ji, G., and Dong, Z., An MR Brain Images Classifier System via Particle Swarm Optimization and Kernel Support Vector Machine. *Hindawi Publishing Corporation. Sci. World J.*:130134, 2013. <https://doi.org/10.1155/2013/130134>.
- Meng, X., Liu, Y., Gao, X. and Zhang, H., A new bio-inspired algorithm: chicken swarm optimization. In *International Conference in Swarm Intelligence*, 86–94. Springer International Publishing, 2014. [https://doi.org/10.1007/978-3-319-11857-4\\_10](https://doi.org/10.1007/978-3-319-11857-4_10).
- Zadeh, L. A., Fuzzy sets. *Inf. Control.* 8(3):338–353, 1965.
- Deng, Y. Y., and Dai, Q., Discriminative clustering and feature selection for brain MRI segmentation. *IEEE Signal Processing Letters.* 22:573–577, 2015. <https://doi.org/10.1109/LSP.2014.2364612>.

34. Yang, M. S., Lin, K. C. R., Liu, H. C., and Limg, J. F., Magnetic resonance imaging segmentation techniques using batch-type learning vector quantization algorithms. *Magn. Reson. Imaging* 25:265–277. Elsevier, 2007. <https://doi.org/10.1016/j.mri.2006.09.043>.
35. Song, T., Jamshidi, M. M., Lee, R. R., and Huang, M., A Modified Probabilistic Neural Network for Partial Volume Segmentation in Brain MR Image. *IEEE Trans. on Neural Networks*. 18(5):1424–1432, 2007. <https://doi.org/10.1109/TNN.2007.891635>.
36. Haralick, R. M., and Shanmugam, K., Textural features for image classification. *IEEE Transactions on Systems, Man, and Cybernetics*. 3(6):610–621, 1973.